Breaking Cassie's Law for Condensation in a Nanopatterned Slit

Martin Láska
Department of Physical Chemistry, University of Chemical Technology Prague, Praha 6, 166 28, Czech Republic and The Czech Academy of Sciences, Institute of Chemical Process Fundamentals, Department of Molecular Modelling, 165 02 Prague, Czech Republic

Andrew O. Parry
Department of Mathematics, Imperial College London, London SW7 2BZ, United Kingdom

Alexandr Malijevský
Department of Physical Chemistry, University of Chemical Technology Prague, Praha 6, 166 28, Czech Republic and The Czech Academy of Sciences, Institute of Chemical Process Fundamentals, Department of Molecular Modelling, 165 02 Prague, Czech Republic

(Received 7 December 2020; revised 10 February 2021; accepted 1 March 2021; published 26 March 2021)

We study the phase transitions of a fluid confined in a capillary slit made from two adjacent walls, each of which are a periodic composite of stripes of two different materials. For wide slits the capillary condensation occurs at a pressure which is described accurately by a combination of the Kelvin equation and the Cassie law for an averaged contact angle. However, for narrow slits the condensation occurs in two steps involving an intermediate bridging phase, with the corresponding pressures described by two new Kelvin equations. These are characterised by different contact angles due to interfacial pinning, with one larger and one smaller than the Cassie angle. We determine the triple point and predict two types of dispersion force induced Derjaguin-like corrections due to mesoscopic volume reduction and the singular free-energy contribution from nanodroplets and bubbles. We test these predictions using a fully microscopic density functional model which confirms their validity even for molecularly narrow slits. Analogous mesoscopic corrections are also predicted for two-dimensional systems arising from thermally induced interfacial wandering.

DOI: 10.1103/PhysRevLett.126.125701

The equilibrium phases of confined fluids have been the subject of long-standing interest. At the bulk critical point, fluctuations lead to the thermal analog of the Casimir force [1], while at lower temperatures the liquid-gas phase boundary is shifted leading to the phenomenon of capillary condensation [2–5]. By having walls which preferentially adsorb different phases one can also radically alter the nature of the phase equilibria due to interfacial effects [6,7]. Indeed, it is now possible to observe experimentally the condensation in pores of different geometries fabricated using electron beam nanolithography [8]. In the present Letter we discuss the nature of capillary condensation in a slit for which the walls are periodically patterned with two different types of material. This is much richer than that occurring for chemically homogeneous slits since the condensation from gas to liquid may either occur directly or in two steps via an intermediate bridgelike phase. The location of these phase transitions is described by generalized Kelvin equations which involve one of three possible contact angles each associated with meniscus pinning. Only one of these angles is the Cassie angle [9], which lies between the other two, somewhat analogous to contact angle hysteresis [10,11]. By allowing for dispersion forces we predict Derjaguin-like corrections to the Kelvin equations due to volume reduction and the singular free energy of droplets and bubbles adsorbed at the walls.

To begin, we recall the macroscopic Kelvin equation and mesoscopic Derjaguin correction for condensation in a chemically homogeneous slit, made from two infinite planar walls separated by a distance L. The fluid is at pressure p (or, equivalently, chemical potential μ), at a temperature T below the critical point. Confinement changes the liquid-gas phase boundary, which is the pressure when gas condenses to liquid, away from the bulk saturation curve $p_{\rm sat}(T)$. Macroscopically, the shift from $p_{\rm sat}$, at which capillary condensation (cc) occurs is described by the Kelvin equation [12]

$$\delta p_{cc} = \frac{2\gamma\cos\theta}{L}, \tag{1}$$

where θ is the contact angle defined by Young's equation $\gamma_{wg} = \gamma_{wl} + \gamma\cos\theta$ for each semi-infinite wall. Here γ_{wg}, γ_{wl}, and γ are the tensions of the wall-gas, wall-liquid, and liquid-gas interfaces, respectively. For partial wetting the

Kelvin equation is remarkably accurate for L down to tens of molecular length scales. However, for complete wetting ($\theta = 0$), corrections are apparent at the mesoscopic scale. In particular, for systems with dispersion forces the Kelvin equation is modified to [13,14]

$$\delta p_{cc} = \frac{2\gamma}{L - 3\ell}, \tag{2}$$

which includes the Derjaguin correction allowing for the thickness ℓ of the liquid layer adsorbed at each wall in the gaslike phase. This is very well approximated as $\ell = (2A/\delta p)^{-1/3}$, where A is the Hamaker constant and $\delta p = p_{\rm sat} - p$, corresponding to the wetting layer thickness at a single wall [15,16].

We now turn to a heterogeneous slit where the walls are made of two materials arranged into a periodic array of stripes of width H_1 and H_2, each characterized by different contact angles θ_1 and θ_2. The two walls are adjacent with translation invariance assumed along the stripes (i.e., the stripes on the opposing walls are exactly aligned). We assume that material 1 preferentially adsorbs liquid relative to material 2 so that $\theta_1 < \theta_2$. The condensation in this capillary may happen by two mechanisms similar to that if there is a single stripe on each surface [17] or between geometrically structured walls [18,19]. For wide slits it occurs via a single first-order phase transition from a gaslike to liquidlike phase similar to that for a chemically homogeneous slit. However, if the slit is sufficiently narrow, condensation happens in two steps via an intermediate phase in which liquid bridges locally condense between the stripes of the more wettable material 1 (see Fig. 1). We first derive the generalized, macroscopic Kelvin equations which determine the phase boundaries for each type of condensation:

One-step condensation.—The pressure at which gas condenses to liquid is determined by balancing the grand potential Ω per unit length (along the stripe) and over a single period of the two phases. For the gaslike phase $\Omega_g \approx -pHL + 2\gamma_{wg}^{(1)} H_1 + 2\gamma_{wg}^{(2)} H_2$, where $\gamma_{wg}^{(i)}$ are the wall-gas tensions for each material and $H = H_1 + H_2$. Similarly, for the liquidlike phase we have $\Omega_l \approx -p^\dagger HL + 2\gamma_{wl}^{(1)} H_1 + 2\gamma_{wl}^{(2)} H_2$, where $p^\dagger$ is the pressure of the metastable bulk liquid and $\gamma_{wl}^{(i)}$ are two wall-liquid surface tensions. Balancing the grand potentials determines that the value of $p - p^\dagger \approx \delta p_{cc}$ at which (single step) capillary condensation occurs is given by

$$\delta p_{cc} = \frac{2\gamma \cos\theta_{\rm cas}}{L}, \tag{3}$$

which is unaltered if the stripes are not perfectly adjacent, i.e., if the upper wall (say) in Fig. 1 is shifted or indeed, rotated so the stripes are no longer parallel. This is the obvious generalization of the standard Kelvin equation and identifies that the appropriate contact angle appearing in it is the familiar Cassie angle [9],

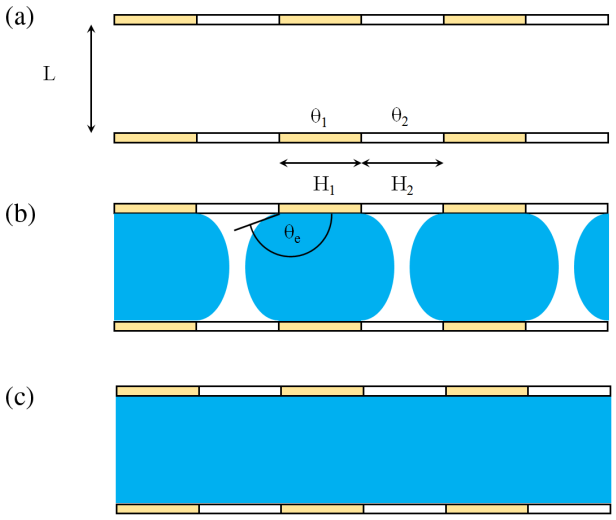

FIG. 1. Schematic illustration of (a) gaslike, (b) liquid bridge (blue), and (c) liquidlike configurations in a periodic slit. The edge contact angle θ_e is highlighted, drawn here for $p > p_{\rm sat}$.

$$\cos\theta_{\rm cas} = f_1 \cos\theta_1 + f_2 \cos\theta_2, \tag{4}$$

where $f_i = H_i/H$ is a fraction of the wall area occupied by each material. Viewed in terms of phase separation, $\theta_{\rm cas}$ is the angle that a circular meniscus of radius $R = \gamma/\delta p_{cc}$, which separates the coexisting phases, meets both walls at one of the edges between the two materials.

Two-step condensation.—In this case, there are two phase boundaries corresponding to a pressure shift δp_{gb}, where the gas phase locally condenses to a bridge phase, and a second δp_{lb} (at higher pressure) when the bridge phase condenses to liquid. These are determined by matching the grand potential of a bridge phase Ω_b with Ω_g and Ω_l. In each unit cell the liquid bridge is bounded by two circular menisci of radius $R = \gamma/\delta p$ which are pinned at the edges between the two materials (see Fig. 1). These meet the walls at an edge contact angle θ_e, which is related to the pressure by $\cos\theta_e = L/2R$. The grand potential of the bridge phase is given by $\Omega_b \approx -pA_g - p^\dagger A_l + 2(H_1\gamma_{wl}^{(1)} + H_2\gamma_{wg}^{(2)}) + 2\gamma l_{\rm men}$, where A_g and A_l are the areas occupied by the gas and (metastable) liquid, respectively, and $l_{\rm men}$ is the length of each meniscus. Equating this value with Ω_g and Ω_l determines the pressure shifts as

$$\delta p_{gb} = \frac{2\gamma \cos\theta_{gb}}{L}, \qquad \delta p_{lb} = \frac{2\gamma \cos\theta_{lb}}{L}, \tag{5}$$

where θ_{gb} and θ_{lb} are the values of the edge contact angles at the respective phase transitions given by [20]

$$\cos\theta_1 = \cos\theta_{gb} + \frac{L}{2H_1}\left[\sin\theta_{gb} + \sec\theta_{gb}\left(\frac{\pi}{2} - \theta_{gb}\right)\right] \quad (6)$$

and

$$\cos\theta_2 = \cos\theta_{lb} - \frac{L}{2H_2}\left[\sin\theta_{lb} + \sec\theta_{lb}\left(\frac{\pi}{2} - \theta_{lb}\right)\right], \quad (7)$$

which satisfy $\theta_{gb} < \theta_{\rm cas} < \theta_{lb}$. The phase transition occurring at δp_{lb} is equivalent to the local evaporation of liquid between the less wettable stripes as p is reduced.

Condensation occurs via one step if $\theta_{gb} > \theta_{\rm cas}$ (wide slits) or two steps if $\theta_{gb} < \theta_{\rm cas}$ (narrow slits). The marginal case between these two different mechanisms occurs when $\theta_{gb} = \theta_{lb}$ (equivalent to each being equal to $\theta_{\rm cas}$) and identifies the triple point (T) where the gaslike, liquidlike and bridging phases coexist. This happens when the aspect ratio $a \equiv L/H_1$ takes the value

$$a_T = \frac{2f_2(\cos\theta_1 - \cos\theta_2)}{\sin\theta_{\rm cas} + \sec\theta_{\rm cas}(\frac{\pi}{2} - \theta_{\rm cas})}. \quad (8)$$

In the limit $f_1 = 0$, Eq. (8) reduces to the result pertinent to a parallel plate geometry in which there is just a single, adjacent stripe, of material 1 on each wall [17]. If the aspect ratio is greater than this value the condensation occurs via one step. We illustrate this in Fig. 2, where we plot the three contact angles appearing in the generalized Kelvin equations for a *maximum contrast* slit ($\theta_1 = 0$ and $\theta_2 = \pi$) as a function of the aspect ratio a for equal stripe widths $H_1 = H_2$.

These macroscopic arguments do not allow for the direct influence of dispersion forces. Recall that for a homogeneous slit, they may be safely ignored for partial wetting but lead to the Derjaguin correction (2) for complete wetting. The situation is somewhat richer for the patterned slit. If both materials are partially wet, then, as for the homogeneous case, we anticipate that the Kelvin equations for one and two step condensation remain accurate down to molecularly narrow slits. However, if one of the materials is wet (or dry) then the influence of the long-range forces becomes important at the mesoscopic scale. This is most transparent when we consider the maximum contrast slit described above where material 1 is completely wet and material 2 is completely dry. In the gaslike phase each stripe of material 1 is wet by a drop of liquid and, in the liquidlike phase, each stripe of material 2 is wet by a bubble of gas. The volumes of these, which would become macroscopic as H_1, H_2, and L increase need to be taken into account when we consider, for example, the value of the pressure shift δp_T at the triple point. The shape of these drops and bubbles is determined by the intermolecular forces and can be calculated using interfacial Hamiltonian methods [21]. The pressure shift at the triple point for the maximum contrast slit is then modified from Eq. (3) to

$$\delta p_T = \frac{2\gamma\cos\theta_{\rm cas}}{L - \frac{\pi}{4}(f_1 l_D + f_2 l_B)}, \quad (9)$$

where $l_D = (A_1/2\gamma)^{1/4}\sqrt{H_1}$ is the maximum thickness of the wetting drop and $l_B = (A_2/2\gamma)^{1/4}\sqrt{H_2}$ is the maximum thickness of the drying bubble. Here A_1 and A_2 are the Hamaker constants for each material. Since at the triple point H_1 and H_2 are both of order L, the reduction in the effective slit width is *greater* than that occurring in a homogenous system (since at condensation $\ell \sim L^{1/3}$). Note that as H_2 is reduced to a value $\propto \ln H_1$ the drops coalesce to cover the whole surface corresponding to a first-order wetting transition at which $\theta_{\rm cas}$ vanishes [22]. For smaller values of H_2 both walls are completely wet and the location of the single step condensation is described by the usual Derjaguin correction (2).

The location of the triple point for the maximum contrast slit is most subtle when the area fractions are equal, $f_1 = f_2 = 1/2$, since in that case the wall is overall neutral, $\theta_{\rm cas} = \pi/2$. The Kelvin-Cassie equation (3) predicts that single step condensation occurs at $p_{\rm sat}$, while Eq. (8) predicts that the triple point occurs for $a_T = 1$ (see Fig. 2). This macroscopic prediction for a_T is easy to understand. The menisci which bound the liquid bridges are flat with a free-energy cost of $2\gamma L$ per unit cell. For the gaslike (liquidlike) phase this must be compensated by having a drop of liquid (bubble of gas) coat the wet (dry) stripes which carries with it a macroscopic free-energy cost of $2\gamma H_1$ per unit cell. Thus, purely macroscopically, the triple point must occur for $L = H_1$. When we include dispersion forces, however, the surface free energy of a

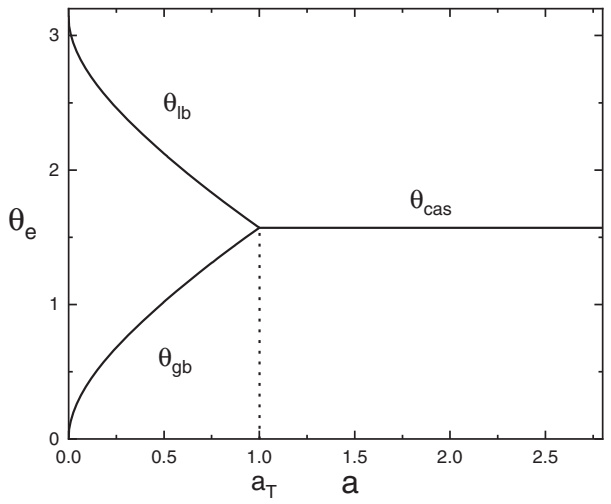

FIG. 2. Contact angles appearing in the macroscopic Kelvin equations for one step and two step condensation [see Eqs. (3) and (5)] in a maximum contrast slit ($\theta_1 = 0$ and $\theta_2 = \pi$) as a function of the aspect ratio $a = L/H_1$. For equal area fractions, $f_1 = f_2 = \frac{1}{2}$, the triple point occurs at $a_T = 1$.

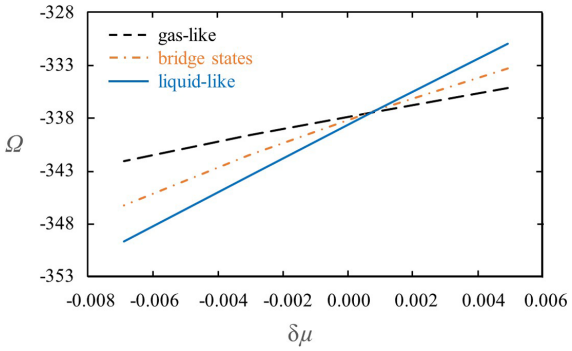

FIG. 3. DFT results determining the triple point for the maximum contrast slit with $H_1 = H_2 = 40\sigma$ and slit width $L = 48\sigma$. The graph shows that the grand potential (per unit length, over one cell and in units ε of the fluid-fluid potential strength [25]) as a function of the undersaturation $[\delta\mu = (\mu_{\rm sat} - \mu)/\varepsilon]$ for the gaslike, liquidlike, and bridge configurations all intersect at a value of the chemical potential close to, but slightly away from bulk saturation. The triple point aspect ratio $a_T = 1.2$, below which Cassie's law breaks down, is slightly above the macroscopic prediction $a_T = 1$ in accordance with Eq. (11).

liquid drop, and similarly for the gas bubble, contains a Casimir-like contribution $\sqrt{2A_1/\gamma}\ln(H_1/\sigma)$, where σ is a molecular diameter. Taking these into account determines the higher-order contribution to Eq. (9) when the walls are neutral:

$$\delta p_T = \sqrt{2\gamma}(\sqrt{A_1} - \sqrt{A_2})\frac{\ln L/\sigma}{L^2}; \quad \text{for } \theta_{\rm cas} = \frac{\pi}{2}. \tag{10}$$

This small shift therefore owes its origin to the difference in the strengths of the dispersion forces; we note that it is larger than the shift $\delta p_{cc} = 2A/L^3$ for a homogeneous slit when $\theta = \pi/2$. Similarly, for the aspect ratio we find

$$a_T = 1 + \frac{\sqrt{A_1} + \sqrt{A_2}}{\sqrt{2\gamma}}\frac{\ln L/\sigma}{L} + \cdots, \tag{11}$$

which approaches unity as the slit width increases.

We have tested the above prediction for the value of a_T for the maximum contrast slit using a microscopic density functional theory (DFT) that we use to determine the equilibrium density profiles and free-energies of stable and metastable phases [23]. These are obtained by minimizing a grand potential functional

$$\Omega[\rho] = \mathcal{F}[\rho] + \int d\mathbf{r}\rho(\mathbf{r})[V(\mathbf{r}) - \mu], \tag{12}$$

where $V(\mathbf{r})$ is the external potential modelling the long-ranged interaction from the patterned walls and $\mathcal{F}[\rho]$ is the intrinsic free-energy functional for which we use Rosenfeld's fundamental measure theory [24] (see Supplemental Material [25]). We have determined the phase coexistence for system sizes ranging from $L = 10\sigma$ to $L = 110\sigma$ and for different stripe widths $H_1(= H_2)$. Figure 3 shows the equilibrium grand potential versus the undersaturation close to the triple point for $H_1 = H_2 = 40\sigma$ and $L = 48\sigma$. The three coexisting density profiles are shown in Fig. 4. Finally, in Fig. 5 we plot the triple point aspect ratio as a function of slit width which shows that, as predicted, the value tends to unity as L increases. In the inset we show that the deviation from unity is extremely well described by the $\ln L/L$ correction in accordance with the prediction (11).

In three dimensions these results are not affected significantly by thermal fluctuations where their only influence is to round the bridging transitions associated with two-step condensation over a pressure range $\mathcal{O}(e^{-\gamma LH/k_BT})$. Thermal fluctuations are much more important in two dimensions for systems with short-ranged forces. Here, a simple realization of the neutral wall is an Ising strip of width L, where the surface spins are fixed to be up and down each over a distance H_1. Single step condensation between predominately down-spin (analogous to gas) and up-spin (liquid) phases, occurs at zero bulk field, $h = 0$, rounded over a scale $\mathcal{O}(e^{-\gamma L/k_BT})$, while bridging occurs away from $h = 0$ (except at the triple point) and is rounded over a scale $\mathcal{O}(1/LH_1)$ [26]. Interfacial wandering in all three phases leads to similar mesoscopic corrections to those predicted for dispersion forces. These can be determined using random walk arguments and interfacial models [27–29]. For the gas phase, the entropic repulsion of the interfaces that bound

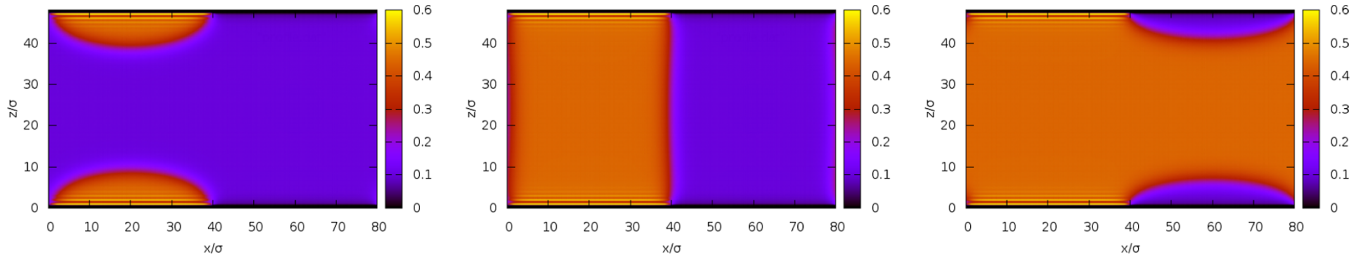

FIG. 4. Equilibrium density profiles (over one period) for coexisting states at the triple point for a maximum contrast slit with $H_1 = H_2 = 40\sigma$ and $L = 48\sigma$. Left and right correspond to gaslike and liquidlike phases for which liquid droplet and gas bubbles are visible, while the center plot corresponds to the bridge state with a near flat meniscus.

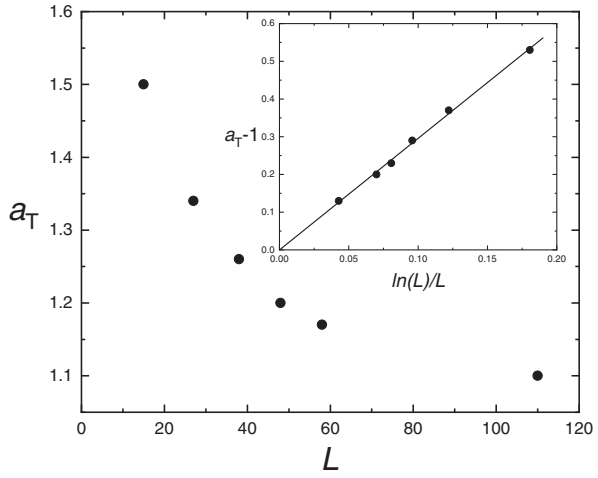

FIG. 5. DFT results of the triple point aspect ratio of a maximum contrast slit for increasing slit width (in units of σ) showing the approach to the macroscopic result $a_T = 1$. The inset shows that the mesoscopic result (11) is accurate down to molecularly narrow slits with $L \approx 15\sigma$.

the liquid drops from the walls leads to a partition function (per unit cell and at $h = 0$) given by $Z_g \approx e^{-2\gamma H_1/k_BT}/H_1^3$ and similarly for the liquid phase. For the bridge, on the other hand $Z_b \approx \mathrm{e}^{-2\gamma L/k_BT}/L$ arising from the wandering of the two near flat menisci. Balancing the free energies determines that a pseudo triple point occurs at $h = 0$ when the aspect ratio is $a_T \approx 1 + (k_BT/\gamma)(\ln L/L)$. This may be checked numerically and may even be amenable to exact analysis [30–33].

In this Letter, we have shown that the locations of one-step and two-step capillary condensation in patterned slits are described by Kelvin equations involving three possible contact angles, only one of which is the Cassie angle θ_{cas} for which we give an explicit geometrical interpretation. However, for narrow slits Cassie's law is broken and two-step condensation is characterized by different angles which arise from meniscus pinning. The pinning associated with these angles not only determines the phase equilibria but will also have a strong influence on metastability relevant to experimental studies and may well underpin the phenomena of contact angle hysteresis. Mesoscopic Derjaguin-like corrections are significantly larger than those for condensation in homogenous slits and are predicted in both two and three dimensions.

This work was financially supported by the Czech Science Foundation, Project No. GA 20-14547S. VIMMP project has received funding from the European Union's Horizon 2020 research and innovation program under Grant Agreement No. 760907.

[1] C. Hertlein, L. Helden, A. Gambassi, S, Dietrich, and C. Bechinger, Nature (London) **451**, 172 (2008).
[2] M. E. Fisher and H. Nakanishi, J. Chem. Phys. **75**, 5857 (1981).
[3] R. Evans, P. Tarazona, and U. Marini Bettolo Marconi, J. Chem. Phys. **84**, 2376 (1986).
[4] R. Evans, J. Phys. Condens. Matter **2**, 8989 (1990).
[5] D. Henderson, *Fundamentals of Inhomogeneous Fluids* (Dekker, New York, 1992).
[6] A. O. Parry and R. Evans, Phys. Rev. Lett. **64**, 439 (1990).
[7] K. Binder, D. Landau, and M. Müller, J. Stat. Phys. **110**, 1411 (2003).
[8] L. Bruschi, G. Mistura, L. Prasetyo, D. D. Do, M. Dipalo, and F. De Angelis, Langmuir **34**, 106 (2018).
[9] A. B. D. Cassie, Discuss. Faraday Soc. **3**, 11 (1948).
[10] P. de Gennes, F. Brochard-Wyart, and D. Quèrè, *Capillarity and Wetting Phenomena: Drops, Bubbles, Pearls, Waves* (Springer, New York, 2013).
[11] D. Quèrè, Annu. Rev. Mater. Res. **38**, 71 (2008).
[12] W. Thomson, Philos. Mag. **42**, 448 (1871).
[13] B. V. Derjaguin, Acta Phys. Chem. **12**, 181 (1940).
[14] R. Evans and U. Marini Bettolo Marconi, Chem. Phys. Lett. **114**, 415 (1985).
[15] R. Lipowsky, Phys. Rev. B **32**, 1731 (1985).
[16] S. Dietrich, in *Phase Transitions and Critical Phenomena*, edited by C. Domb and J. L. Lebowitz (Academic, New York, 1988), Vol. 12.
[17] M. Láska, A. O. Parry, and A. Malijevský, Phys. Rev. Lett. **124**, 115701 (2020).
[18] G. Chmiel, K. Karykowski, A. Patrykiejew, W. Rżysko, and S. Sokołowski, Mol. Phys. **81**, 691 (1994).
[19] P. Röcken, A. Somoza, P. Tarazona, and G. Findenegg, J. Chem. Phys. **108**, 8689 (1998).
[20] A. Malijevský, A. O. Parry, and M. Pospíšil, Phys. Rev. E **96**, 020801(R) (2017).
[21] A. Malijevský, A. O. Parry, and M. Pospíšil, Phys. Rev. E **96**, 032801 (2017).
[22] A. Malijevský, A. O. Parry, and M. Pospíšil, Phys. Rev. E **99**, 042804 (2019).
[23] R. Evans, Adv. Phys. **28**, 143 (1979).
[24] Y. Rosenfeld, Phys. Rev. Lett. **63**, 980 (1989).
[25] See Supplemental Material at http://link.aps.org/supplemental/10.1103/PhysRevLett.126.125701 for details of the DFT model.
[26] V. Privman and M. E. Fisher, J. Stat. Phys. **33**, 385 (1983).
[27] M. E. Fisher, J. Stat. Phys. **34**, 667 (1984).
[28] A. O. Parry and R. Evans, J. Phys. A **25**, 275 (1992).
[29] P. Jakubczyk, M. Napiórkowski, and A. O. Parry, Phys. Rev. E **74**, 031608 (2006).
[30] K. Binder, D. Landau, and M. Muller, J. Stat. Phys. **110**, 1411 (2003).
[31] M. Zubaszewska, A. Gendiar, and A. Drzewinski, Phys. Rev. E **86**, 062104 (2012).
[32] D. B. Abraham, F. H. L. Essler, and A. Maciołek, Phys. Rev. Lett. **98**, 170602 (2007).
[33] D. B. Abraham and A. Maciołek, Phys. Rev. Lett. **105**, 055701 (2010).